Biophysical Journal

Supporting Material

Tuning RNA Flexibility with Helix Length and Junction Sequence

Julie L. Sutton[1] and Lois Pollack[1,*]

[1]School of Applied and Engineering Physics, Cornell University, Ithaca, New York

Supporting Material

E_{FRET} Simulations

To assist in interpreting the E_{FRET} for our RNA constructs we used tools developed elsewhere(1) to model the sterically accessible volume (AV) of the dyes attached to RNA as in reference (2). Briefly, .pdb files of RNA structures were input to the FRET_nps program developed in (1) and the C5 atom of the desired base was chosen as attachment point for the dye linker. We used ref. (2)'s values for the linker length (L_{link}) and width (w_{link}) and dye radii (R_{dye}). These values are provided in Table S1. As in ref (2), the accessible volume of three different dye radii were combined to account for the different dye dimensions, and the AV of Cy5 was rotated by an extra 20 degrees about the helical axis to account for the dye's asymmetric nature.

To compare simulations to experiment, we must account for experimental correction factors as well as the correct averaging regime. We chose to average simulated FRET efficiencies assuming fast orientational dye dynamics, but slow inter-dye distance fluctuations (2-4) so that:

$$\mathcal{E}_\gamma = \frac{1}{mn}\sum_{j=1}^{m}\sum_{i=1}^{n}\mathcal{E}_{\gamma,ij}$$

Where $\mathcal{E}_\gamma$ is the gamma-corrected FRET efficiency given by:

$$\mathcal{E}_{\gamma,ij} = \frac{1+\epsilon(R_{ij}/R_0)^6}{1+(1+\epsilon)(R_{ij}/R_0)^6}$$

assuming no crosstalk of acceptor signal into donor channel. R_{ij} is the distance between points R_i within the acceptor AV and R_j within the donor AV, R_0 is the Forster radius (52Å for this dye pair (2)), and ϵ is a correction factor to account for donor cross talk into the acceptor channel (3). Finally, $\mathcal{E}_\gamma$ is related back to the measured E_{FRET} using:

$$\mathcal{E}_\gamma = \frac{E_{FRET}}{E_{FRET}+\gamma(1-E_{FRET})}$$

where $\gamma = \eta_A\phi_A/\eta_D\phi_D$, and $\phi_{A,D}$ and $\eta_{A,D}$ are the quantum yields and detection efficiencies of the acceptor and donor, respectively. Values for $\phi_{A,D}$ were assumed to be the same as in (2), while the ratio of η_A/η_D was measured using the method described in the Supporting Appendix of (5). Finally, the cross-talk correction factor, β, was measured as the ratio of photon counts recorded in the acceptor channel to those in the donor channel from sample containing only Alexa 488. The factor ϵ, defined in (3) equals β/γ. For our microscope, we found β = 0.027, and γ = 1.2.

Differences in fluorophore accessible volume for 12 and 24 bp helices

Label sites were designed to maintain a fixed distance (8bp) from the junction for both 12 and 24bp helix constructs in order to keep the dye environments comparable between different constructs. Since the above method of modeling dye positions requires a known RNA structure, we used the Nucleic Acid Builder (NAB) web server (6) to generate structures where the junction and helices are all A-form. This structure is most likely found for the construct containing poly(A) junctions, at high $MgCl_2$ concentration. We cannot easily compare data to simulations at other salt concentrations since junction conformations are unknown and the RNA conformations are dynamic. We find that the simulated AVs lead to an E_{FRET} difference of 0.067 for the 12 and 24bp helices since the 24bp helix restricts the AV of the dyes relative to the 12bp helix (Figure S1, Table S2), but this difference is not observed experimentally at high [$MgCl_2$]. Because previous experiments validated the assumption of freely rotating dyes (2), it is likely that the actual dye environments are more similar than the calculation suggests. Others report that this modeling method has some discrepancies with molecular dynamics simulations (2) and does not account for interactions between the RNA and the fluorophore. Both Alexa 488 and Cy5 contain negative charges at pH7, which may further restrict their accessible volume. In either case, we expect that any differences between dye environments should be exaggerated at extreme salt concentrations. However, our FRET data only shows differences between constructs of different helix lengths at intermediate salt concentrations. Thus it is unlikely that differences between dye environments alone can explain the observed differences in E_{FRET} between 12 and 24bp helices.

Comparison between simulated and experimental E_{FRET}

Despite the lack of agreement between the 12bp AV simulations and the data, the simulations for the 24bp poly(A) construct agree very well with our measurement at high [$MgCl_2$] (E_{FRET} = 0.396 vs. 0.406, Table S2). However, due to the lack of structural information on the RNA junctions, we can only make qualitative comparisons between data and simulation at other salt concentrations. If we assume a salt-independent R_0 and freely rotating dyes, we expect an overall increase in E_{FRET} for the constructs containing poly(U) junctions compared to the A-form junction at low salt (because helices are skewed) and at high salt (since helices can approach one another).

Although the generated A-form structure reflects a coaxial helix conformation, it does not necessarily reflect the minimum possible E_{FRET}. Thus measurements at other salt concentrations that yield E_{FRET} values as low as ~0.34 are still consistent with our model. For example, because dyes are attached internally via a flexible C6 carbon linker, they are offset from the helical axis. As a consequence, the inter-dye distance (and thus the E_{FRET}) is sensitive to both the relative angular orientation of the helices as well as overall RNA conformational relaxation. Therefore it is possible for dyes to be farther apart than in the construct containing the fully stacked junction if one helix is rotated with respect to the other, and the dyes end up on opposite sides of the molecule. For these reasons, caution should be used in interpreting the data; it is not possible to decouple helix approach and rotation through E_{FRET} alone.

Possibility of intramolecular end-to-end stacking

Although intermolecular stacking is not a problem (smFRET measurements are performed on very dilute samples of RNA), the possibility remains that the two tethered RNA helices may stack due to their close proximity. For this stacking to occur, the junction would have to loop out of the way, and thus is most likely to happen when the construct contains the flexible poly(U) junction. To address the question of end-to-end stacking we simulated the E_{FRET} values obtained from a molecule in which the two helices are fully stacked. We again focus on the 24bp duplex, and we used NAB to generate a structure of a 48bp duplex to mimic two 24bp helices stack end-to-end. This structure yields an E_{FRET} of 0.682 (Table S2, 24bp - stacked), which is larger than the range of E_{FRET} values measured for poly(U) junctions, even in 300mM $MgCl_2$ (the most likely condition to exhibit end-to-end stacking). Thus, the most likely cause of the increase in E_{FRET} is the continuous approach of the two helices, rather than end-to-end stacking.

RNA sequences

RNA sequences were chosen to reduce undesired hairpins and heterodimers as described in the main text. Sequences are provided below. Amino-modified dT bases were incorporated instead of uridine at blue color locations in strands 1 and 2, and were used to attach either Alexa Fluor 488 TFP (strand 1) or Cy5 NHS ester (strand 2). The placeholder X is used to represent the junction, which is either U or A.

12bp construct:

1. 5’ GGGAGUA**U**AGGG 3’
2. 5’ GCGA**U**UAGGAGG 3’
3. 5’ CCCUAUACUCCCXXXXXCCUCCUAAUCGC 3’

24bp construct:

1. 5’ GGGAGUA**U**AGGGAAAAGGGAGUCG 3’
2. 5’ GGAACAGGGAUAGCGA**U**UAGGAGG 3’
3. 5’ CGACUCCCUUUUCCCUAUACUCCCXXXXXCCUCCUAAUCGCUAUCCCUGUUCC 3’

Poisson-Boltzmann simulations

We used the Adaptive Poisson Boltzmann Solver (APBS) (7) to simulate the electrostatic potential around isolated RNA duplexes. PDB coordinates of A-form RNA duplexes were created using the Nucleic Acid Builder web server (6) for a 12bp and a 24bp helix, created using sequence 1 above for each construct and its complement. Simulations were done at four different ion concentrations: 20, 50, 100, and 200mM KCl. The input parameters used for APBS were: ion radius = 2Å (K^+ and Cl^-), and the minimum boundary distance, was set to 60Å for 20 and 50mM KCl, and 40Å for the remaining salt concentrations. APBS output was analysed using MATLAB (Figures S11 and S12).

Dye	w_{link} (Å)	L_{link} (Å)	$R_{dye,1}$ (Å)	$R_{dye,2}$ (Å)	$R_{dye,3}$ (Å)
Alexa 488	4.5	20	5	4.5	1.5
Cy5	4.5	22	11	3	1.5

Table S1: parameters from (2) used in AV simulations

	$\mathcal{E}_{\gamma}$, calc	$E_{FRET, AV}$	$E_{FRET, experimental}$ **For poly(A) in 300mM $MgCl_2$**
12bp	0.290	0.329	0.407 ± 0.007
24bp	0.353	0.396	0.406 ± 0.003
24bp - stacked	0.641	0.682	-

Table S2: comparison between experimental E_{FRET} and AV simulation for RNA constructs.

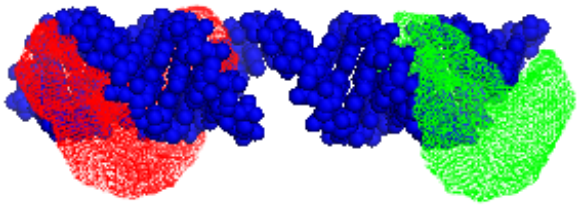

(a) 12bp

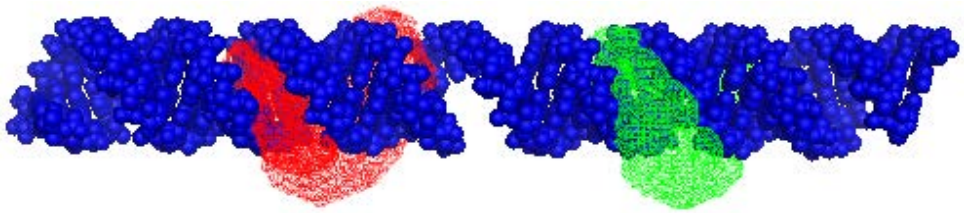

(b) 24bp

Figure S1. Surface representation of accessible dye positions, for Alexa 488 (green) and Cy5 (red) around A-form RNA (blue) for (a) a 12bp and (b) a 24bp RNA helix. Simulations were performed using software developed by (1). Image was generated using PYMOL.

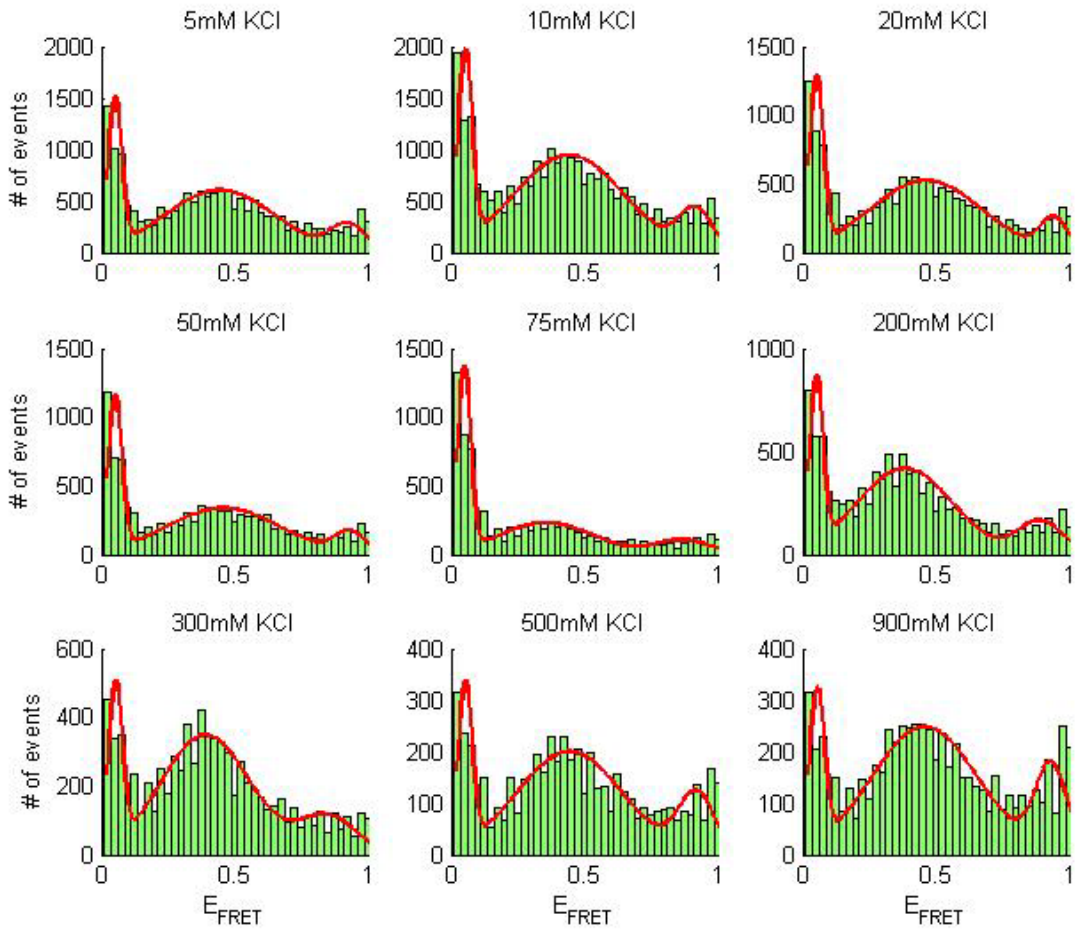

Figure S2. Example histograms (green) fit to 3 gaussians (red) for RNA constructs with 12bp helices and poly(A) junctions in varying [KCl]. Data was truncated for $E_{FRET} \leq 0.02$.

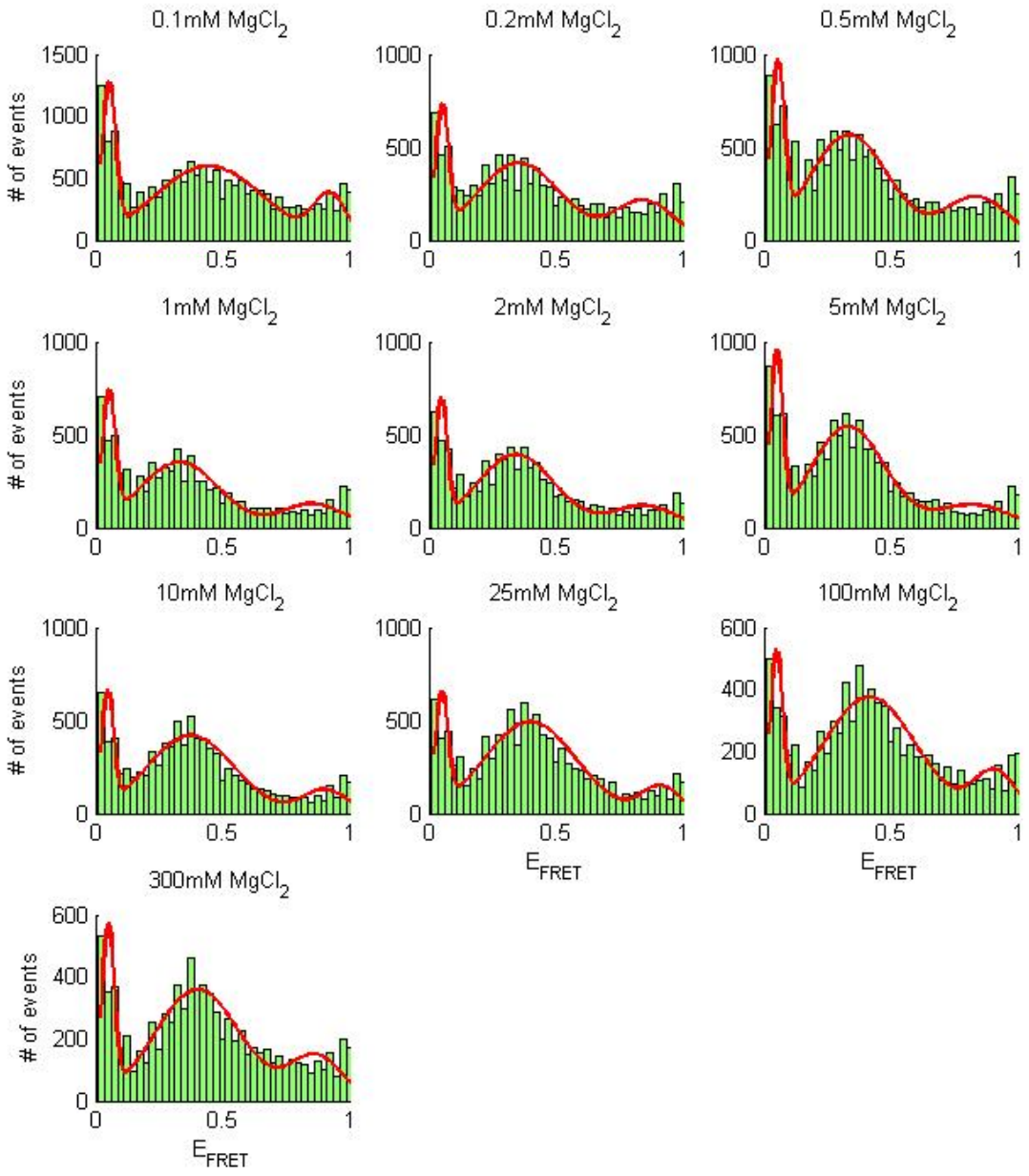

Figure S3. Example histograms (green) fit to 3 gaussians (red) for RNA constructs with 12bp helices and poly(A) junctions in varying [$MgCl_2$]. Data was truncated for $E_{FRET} \leq 0.02$.

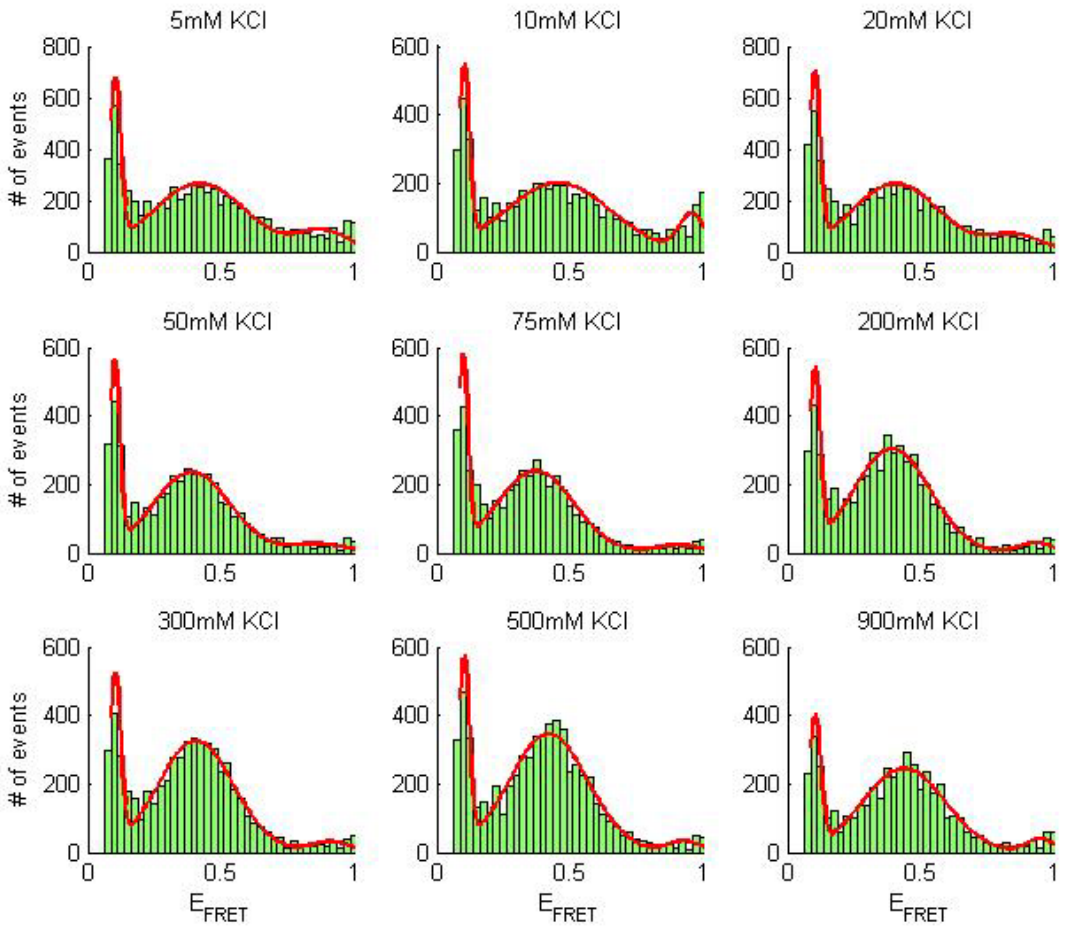

Figure S4. Example histograms (green) fit to 3 gaussians (red) for RNA constructs with 24bp helices and poly(A) junctions in varying [KCl]. Data was truncated for $E_{FRET} \leq 0.08$.

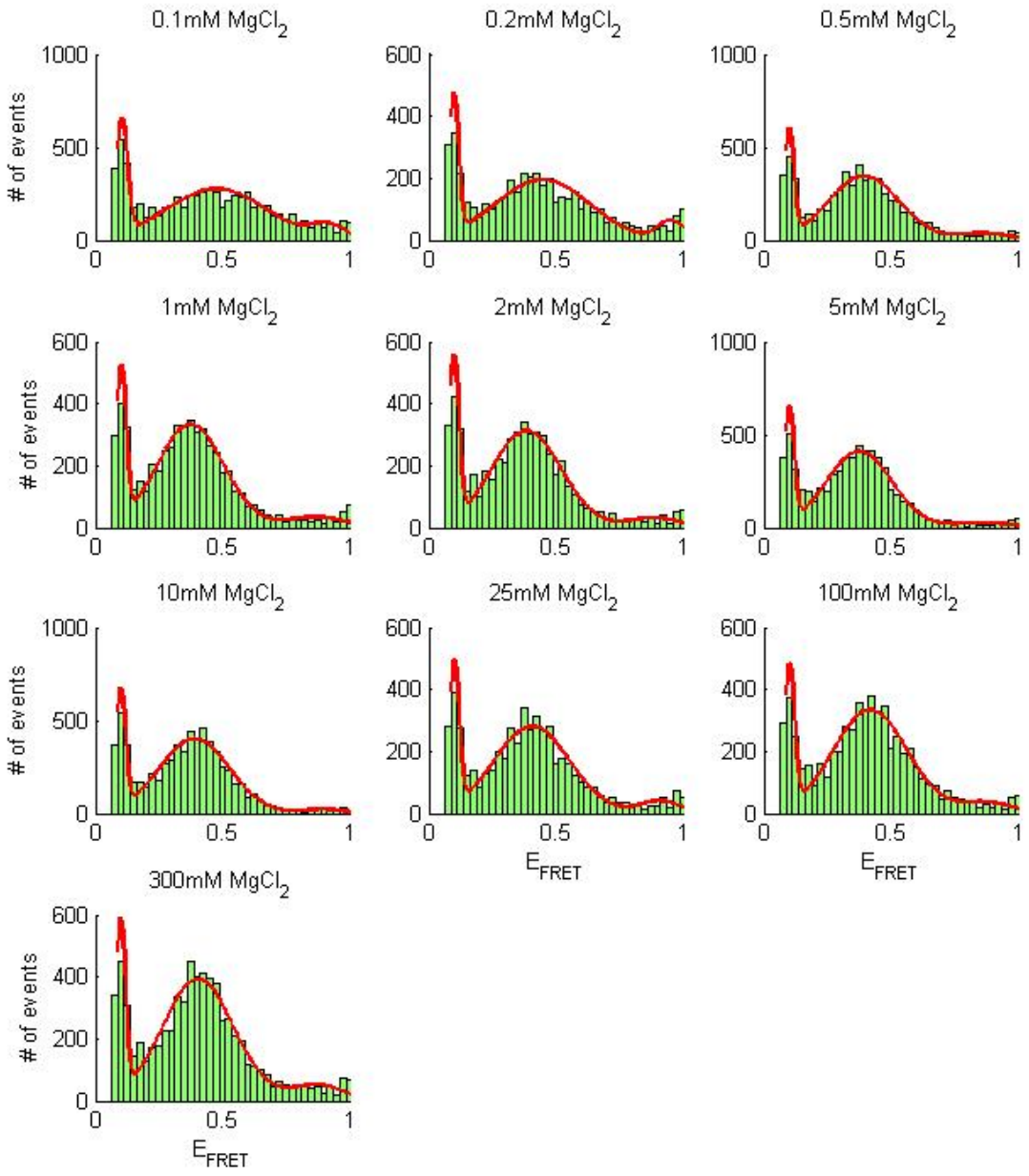

Figure S5. Example histograms (green) fit to 3 gaussians (red) for RNA constructs with 24bp helices and poly(A) junctions in varying [$MgCl_2$]. Data was truncated for $E_{FRET} \leq 0.02$.

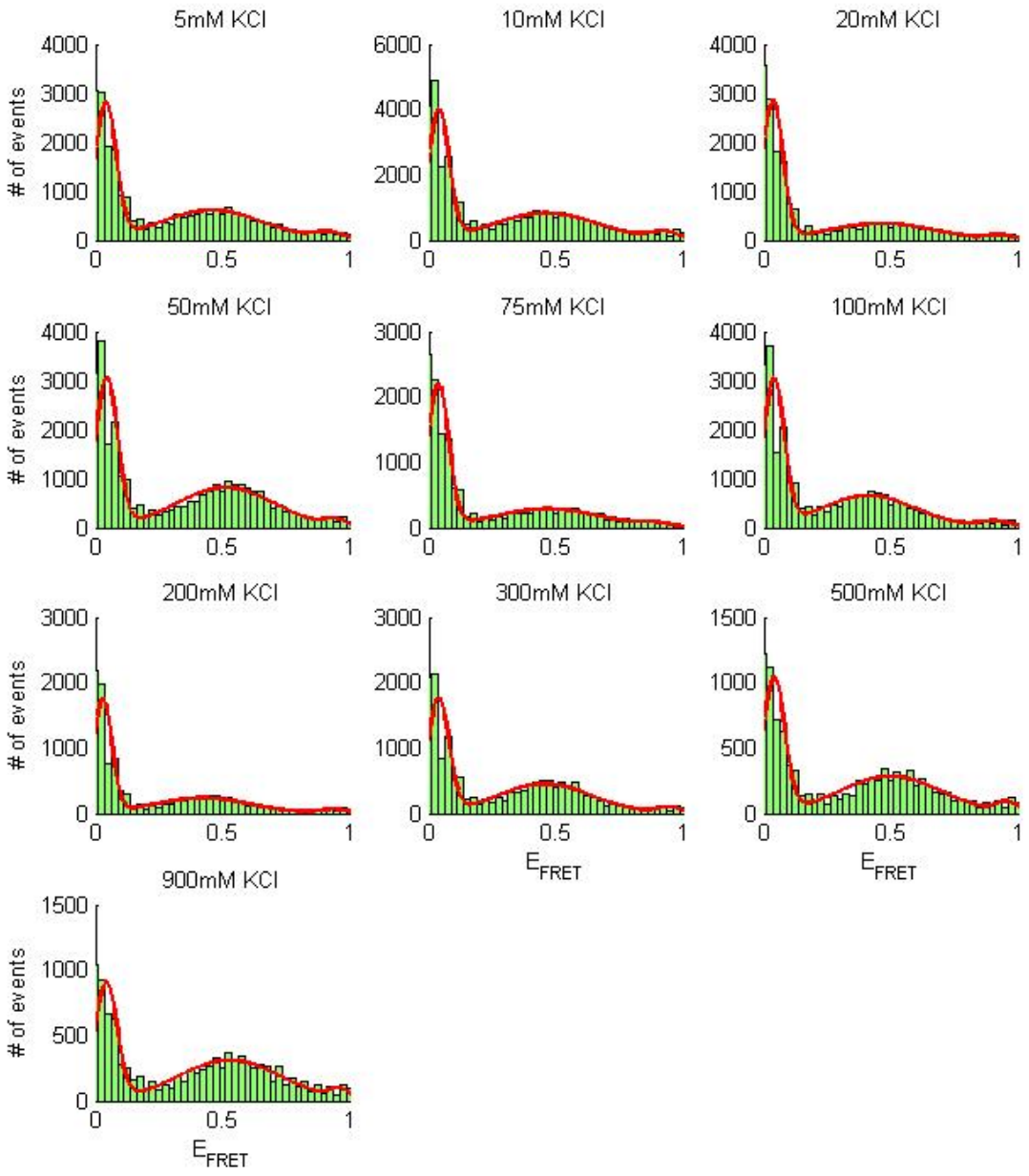

Figure S6. Example histograms (green) fit to 3 gaussians (red) for RNA constructs with 12bp helices and poly(U) junctions in varying [KCl].

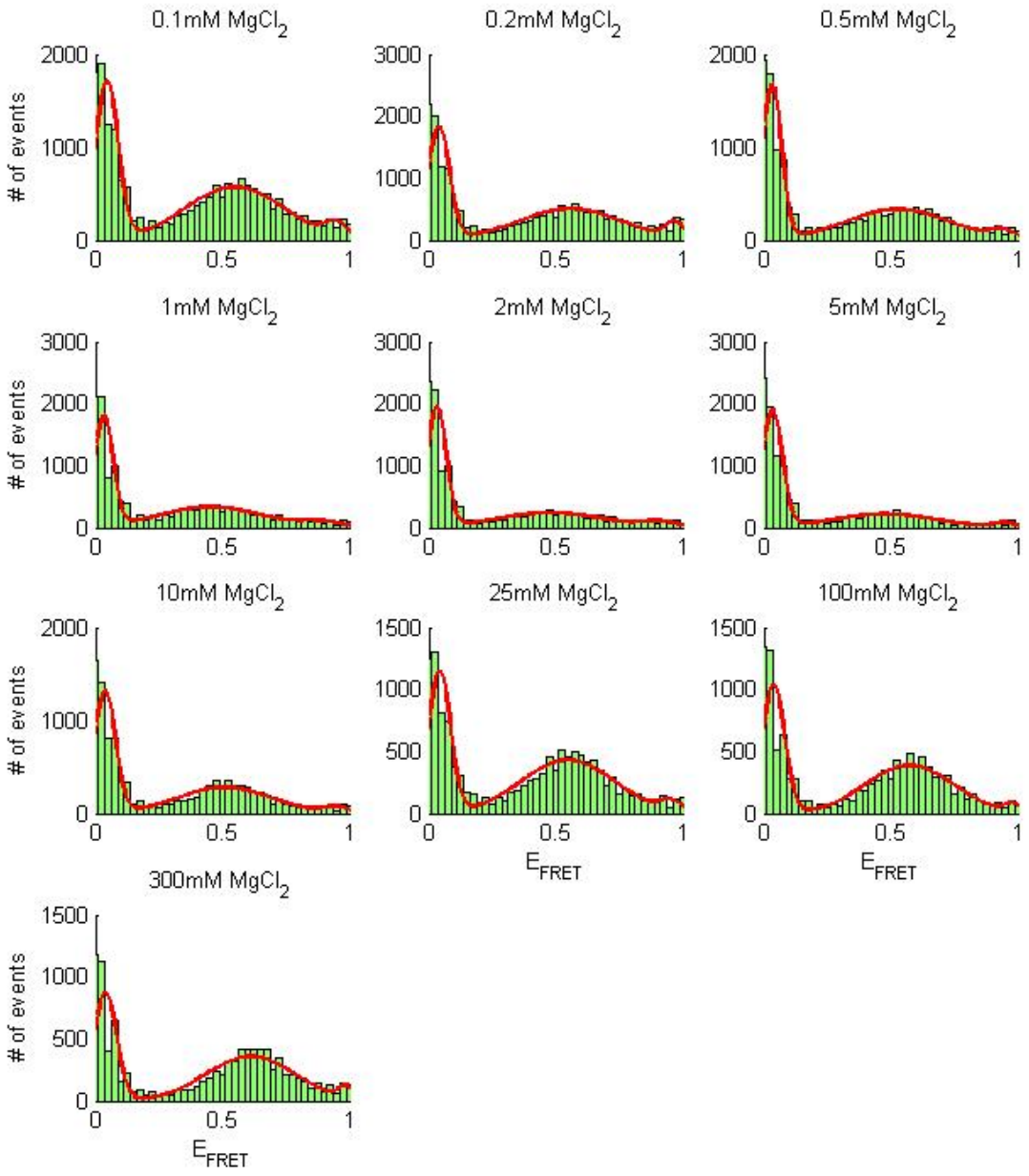

Figure S7. Example histograms (green) fit to 3 gaussians (red) for RNA constructs with 12bp helices and poly(U) junctions in varying [$MgCl_2$].

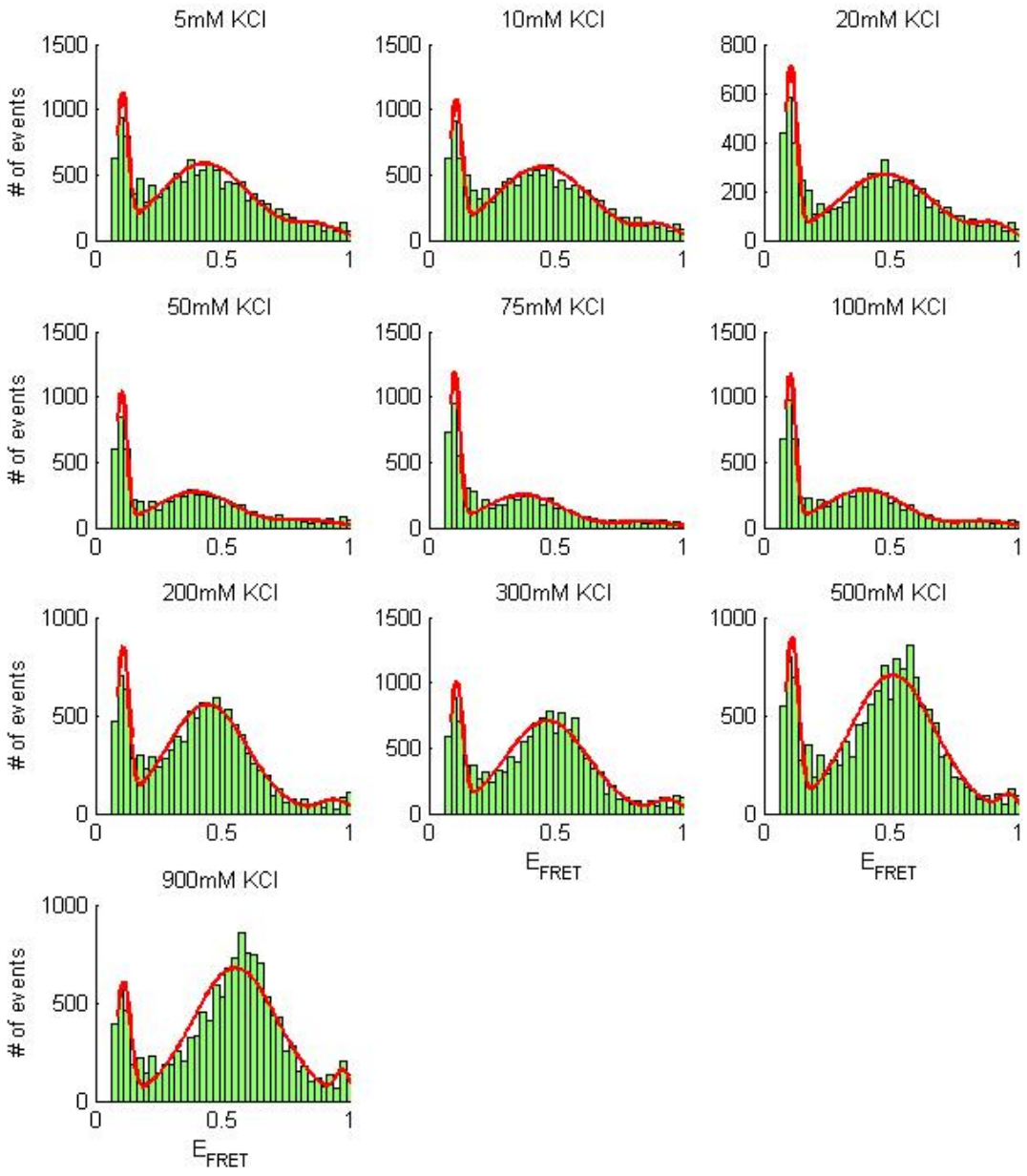

Figure S8. Example histograms (green) fit to 3 gaussians (red) for RNA constructs with 24bp helices and poly(U) junctions in varying [KCl]. Data was truncated for $E_{FRET} \leq 0.08$.

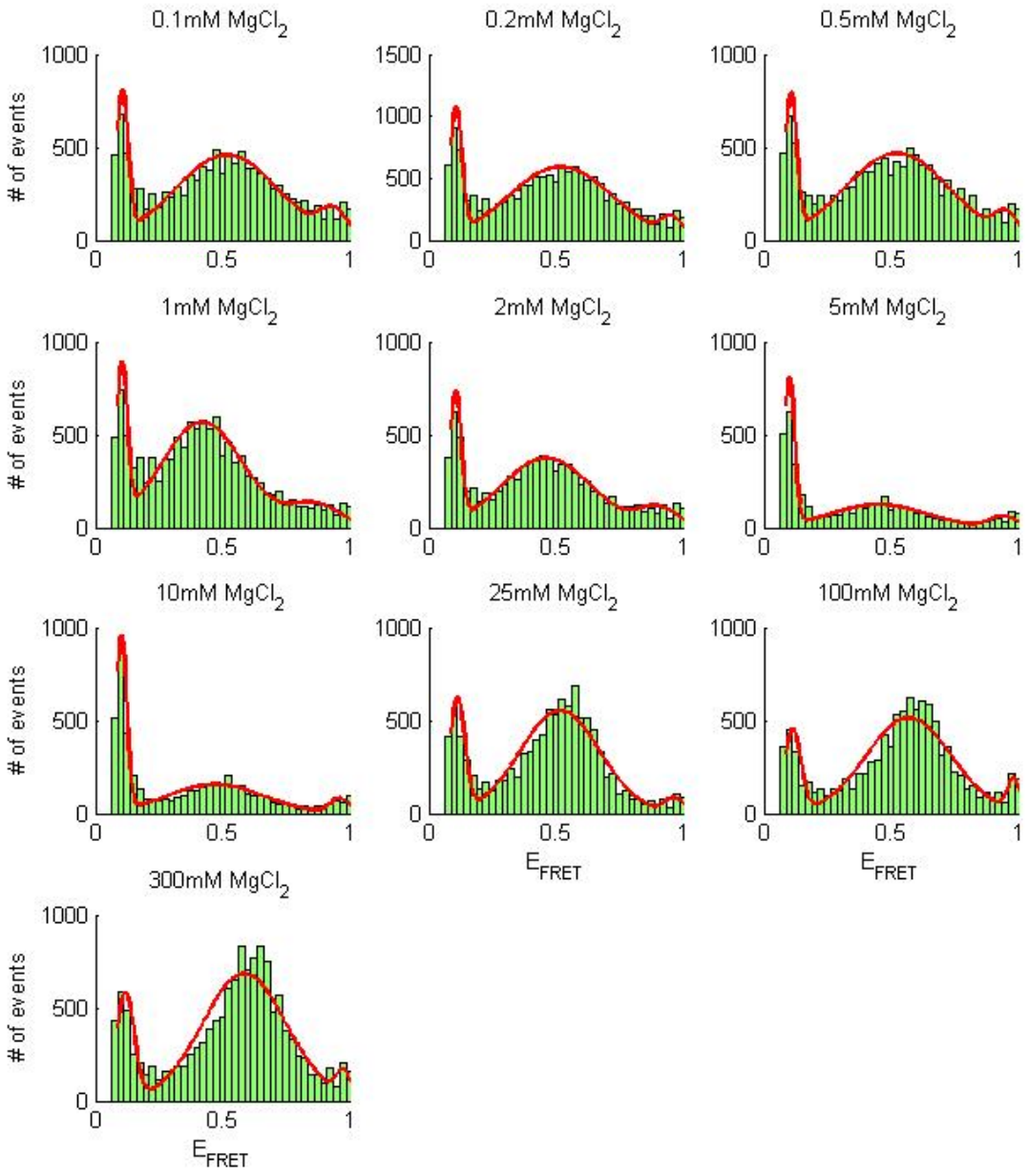

Figure S9. Example histograms (green) fit to 3 gaussians (red) for RNA constructs with 24bp helices and poly(U) junctions in varying [$MgCl_2$]. Data was truncated for $E_{FRET} \leq 0.08$. (a)

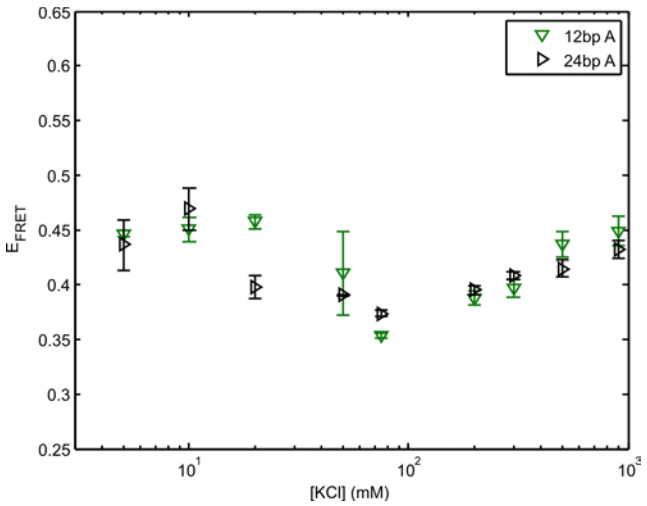

Figure S10: Helix length comparison of poly(A) constructs show similar behavior as constructs with poly(U) junctions. Helix length effects are only observed at intermediate salt concentrations (20-100mM KCl).

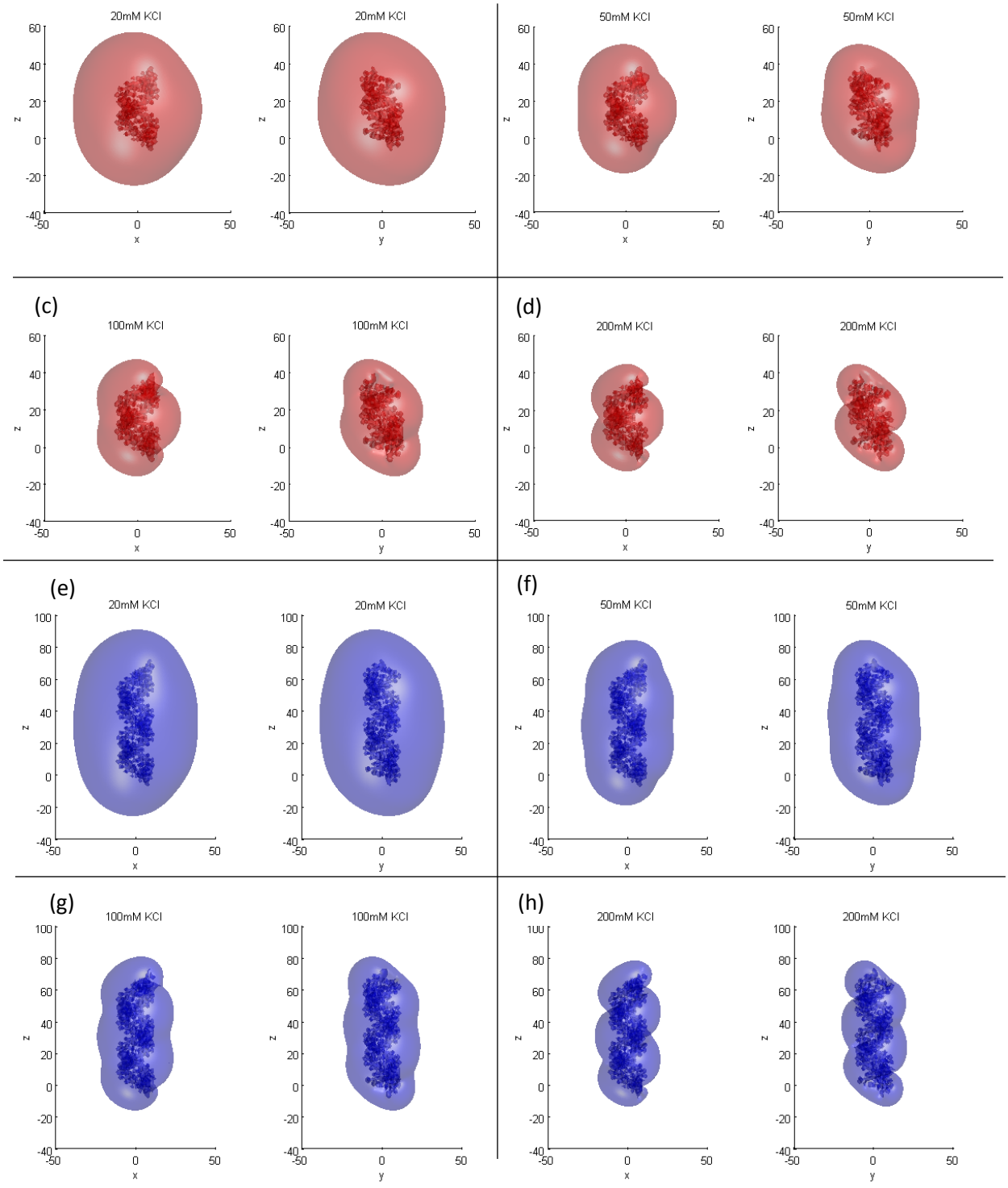

Figure S11: Potentials are visualized using -0.5k_BT/e isosurfaces. Each panel shows the same isosurface from two angles. Panels (a)-(d) show the 12bp helix in increasing [KCl] (20, 50, 100, and 200 mM) and panels (e)-(h) show the 24bp helix in increasing [KCl].

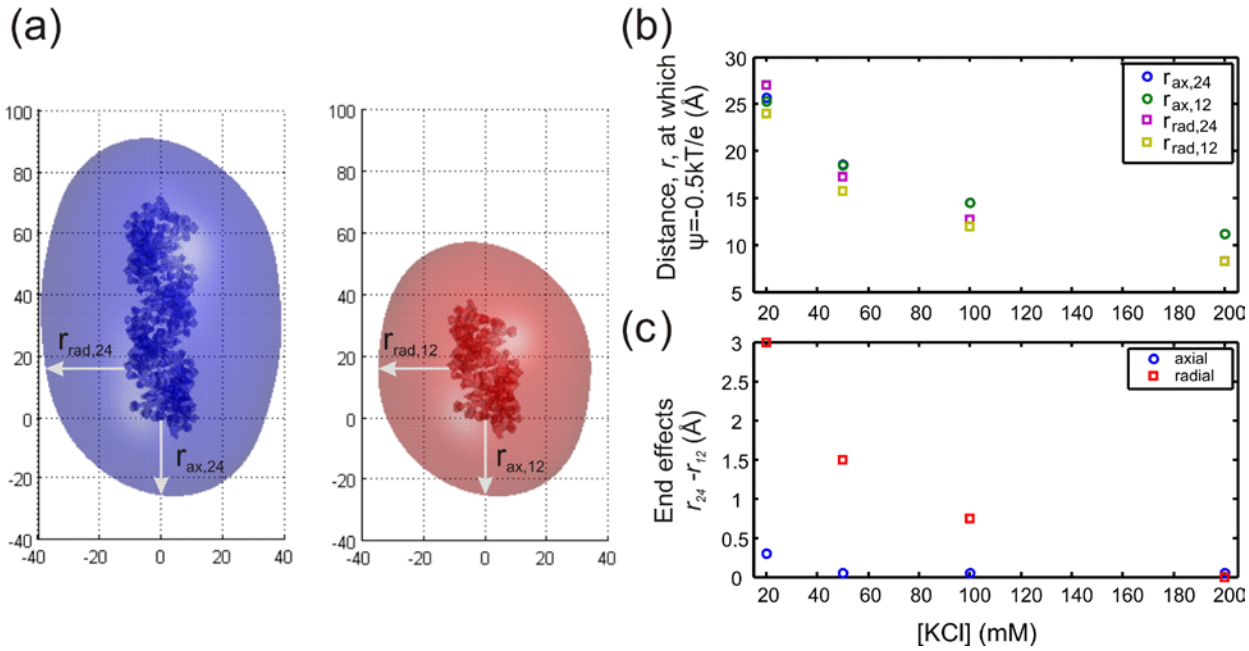

Figure S12: Comparison of end effects for 12 and 24bp helices. (a) Schematic showing relevant lengthscales. To compare the two helix lengths, we cylindrically average the electrostatic potential to get ψ(r,z). We then define a characteristic distances, r_{ax} and r_{rad} as the distance from the RNA surface to where ψ(r,z)=-0.5k_BT/e. (b) Comparison between r_{ax} and r_{rad} for different helix lengths. r_{rad} was measured at z= 16Å which corresponds to halfway along the 12bp helix. (c) End effects as illustrated by the non-zero difference between r_{ax} and r_{rad} for 12 and 24bp helices. Notice how the magnitude of the end effects decreases as [KCl] is increased and how differences in the axial potential are negligible compared to the radial direction.

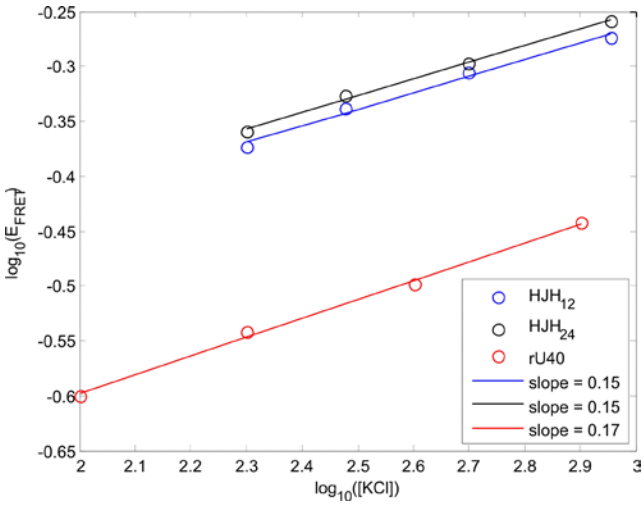

Figure S13: High salt scaling of poly(U)$_{40}$ compared to single-stranded poly(U)$_5$ junction flanked by two helices. Data from Chen et al. (8) was converted into E_{FRET} using their published R_0. On a log-log plot, the scaling of EFRET in KCl is the same (within ~10%).

Literature Cited

1. Muschielok, A., J. Andrecka, A. Jawhari, F. Bruckner, P. Cramer and J. Michaelis 2008. A nano-positioning system for macromolecular structural analysis. Nat. Methods. 5, 965-971.

2. Sindbert, S., S. Kalinin, H. Nguyen, A. Kienzler, L. Clima, W. Bannwarth, B. Appel, S. Muller and C.A. Seidel 2011. Accurate distance determination of nucleic acids via forster resonance energy transfer: Implications of dye linker length and rigidity. J. Am. Chem. Soc. 133, 2463-2480.

3. Gopich, I. V. and A. Szabo.2011.Theory of single-molecule FRET efficiency histograms; In Single-molecule biophysics, John Wiley & Sons, Inc., 245-297.

4. Wozniak, A. K., G.F. Schroder, H. Grubmuller, C.A. Seidel and F. Oesterhelt 2008. Single-molecule FRET measures bends and kinks in DNA. Proc. Natl. Acad. Sci. U. S. A. 105, 18337-18342.

5. Ferreon, A. C., Y. Gambin, E.A. Lemke and A.A. Deniz 2009. Interplay of alpha-synuclein binding and conformational switching probed by single-molecule fluorescence. Proc. Natl. Acad. Sci. U. S. A. 106, 5645-5650.

6. Macke, T. J. and D. A. Case.1997.Modeling unusual nucleic acid structures; Vol. 682. American Chemical Society, 379-393.

7. Baker, N. A., D. Sept, S. Joseph, M.J. Holst and J.A. McCammon 2001. Electrostatics of nanosystems: Application to microtubules and the ribosome. Proc. Natl. Acad. Sci. U. S. A. 98, 10037-10041.

8. Chen, H., S.P. Meisburger, S.A. Pabit, J.L. Sutton, W.W. Webb and L. Pollack 2012. Ionic strength-dependent persistence lengths of single-stranded RNA and DNA. Proc. Natl. Acad. Sci. U. S. A. 109, 799-804.